Model Free Subspace $\mathcal{H}_\infty$ Control for an Autonomous Catamaran

Gabriel H. Elkaim
Department of Computer Engineering
University of California, Santa Cruz
1156 High St., Santa Cruz, CA, 95064
Email: elkaim@soe.ucsc.edu

Bruce R. Woodley, Ph.D.
Principal Systems Engineer
NeoGuide Systems Inc.
104 Cooper Ct.
Los Gatos, CA 95032
Email: brucewoodley@stanfordalumni.org

Robert J. Kelbley
Graduate Student Researcher
University of California, Santa Cruz
1156 High St., Santa Cruz, CA, 95064
Email: rkelbs@soe.ucsc.edu

***Abstract*— An autonomous surface vehicle, based on a Prindle-19 catamaran and substituting a self-trimming vertical wing for the sail, was developed to demonstrate precision guidance and control. This vehicle, the Atlantis, was demonstrated to track straight line segments to better than 0.3 meters (one σ) when already trimmed to sail along a segment, using a Linear Quadratic Gaussian (LQG) controller based on an identified plant using the Observer Kalman Identification (OKID) methods. In this work, a novel controller based on model free subspace $\mathcal{H}_\infty$ control is shown to achieve similar performance levels without building an actual model of the system. These new control methods were tested and implemented on a nonlinear simulation of the catamaran which included realistic wind and current models. The model free control architecture was applied to the simulated catamaran and using Monte Carlo simulations, demonstrated very robust tracking traversal while maintaining a cross-track error of less than one meter throughout the path.**

I. Introduction

The Atlantis, an autonomous wind-propelled catamaran, has previously demonstrated an accuracy better than 0.3 meters (one σ) for line following applications when already trimmed for sail [1]. Atlantis' guidance and control architecture has since been extended allowing precision way-point guided marine navigation [2]. This paper discusses a new extension to Atlantis' control architecture, the addition of a novel direct control design methodology that provides the control response necessary for precision navigation in the presence of unknown wind and water current disturbances.

The connection between system identification experiment design and the designer's control objectives must be taken into consideration when using experimental data in the control design process [5]. With this connection in mind, a direct control technique, "model free subspace $\mathcal{H}_\infty$ control" is applied to the Atlantis providing control design that is directly correlated to experimental system identification data in a model free fashion.

That is, normal system identification techniques require first building a mathematical model of the plant (hence the name: system identification). Using this model, a controller is designed and tested, and then the process is repeated until satisfactory performance is obtained. In a model free technique (often referred to as direct controller design), the controller is created directly from experimental data, avoiding an explicit model formation step.

The model free subspace $\mathcal{H}_\infty$ control methodology utilizes subspace prediction methods directly coupled with $\mathcal{H}_\infty$ performance specifications. The controller provides the Atlantis with precision control capabilities while requiring minimal controller parameter tuning throughout the design process. This $\mathcal{H}_\infty$-optimal feedback controller coupled with a way-point navigation guidance system will allow the Atlantis to perform precision, wind-propelled marine navigation where Autonomous Surface Vehicle (ASV) capabilities are required [10].

Current results are obtained through Monte Carlo simulations using a nonlinear model of the Atlantis, including realistic wind and water current disturbances. Experimental results of Atlantis' guidance and control system are expected by the end of the year.

The key components of the Atlantis are discussed in Section II, including previous results of precise line following control. Next, an overview of model free subspace $\mathcal{H}_\infty$ control is presented in Section III, followed by a discussion of the design parameters chosen for the Atlantis in Section IV. A comparison of LQG and $\mathcal{H}_\infty$ controllers generated from experimental data is provided in Section V. The segmented trajectories (consisting of arcs and lines) used to connect way-points are outlined in Section VI. Monte Carlo simulation results are presented in Section VII and finally a conclusion is provided in Section VIII.

II. The Atlantis

A. System Overview

The Atlantis, pictured in Fig. 1, is an unmanned, autonomous, GPS-guided, wing-sailed sailboat. The Atlantis has demonstrated advanced precision control of a wind-propelled marine vehicle to an accuracy of better than one meter. The prototype is based on a modified Prindle-19 light catamaran.

The wind-propulsion system is a rigid wing-sail mounted vertically on bearings to allow free rotation in azimuth about a stub-mast. Aerodynamic torque about the stub-mast is trimmed using a flying tail mounted on booms joined to the wing.

Fig. 1. Atlantis with wing-sail, January 2001.

This arrangement allows the wing-sail to automatically attain the optimum angle to the wind, and weather vane into gusts without inducing large heeling moments. Modern airfoil design allows for an increased lift to drag ratio (L/D) over a conventional sail, thus providing increased thrust while reducing the overturning moment.

The system architecture is based on distributed sensing and actuation, with a high-speed digital serial bus connecting the various modules together. Sensors are sampled at 100Hz., and a central guidance navigation and control (GNC) computer performs the estimation and control tasks at 5Hz. This bandwidth has been demonstrated to be capable of precise control of the catamaran.

The sensor system uses differential GPS (DGPS) for position and velocity measurements, augmented by a low-cost attitude system based on accelerometer- and magnetometer-triads. Accurate attitude and determination is required to create a synthetic position sensor that is located at the center-of-gravity (CG) of the boat, rather than at the GPS antenna location.

Previous experimental trials recorded sensor and actuator data intended to excite all system modes. A system model was assembled using Observer Kalman System Identification (OKID) techniques [6]. An LQG controller was designed using the OKID model, using an estimator based on the observed noise statistics. Experimental tests were run to sail on a precise track through the water, in the presence of currents, wind, and waves.

B. Previous Line Following Control Results

In order to validate the performance of the controllers and all up system, closed loop control experiments were performed in Redwood City Harbor, California, on January 27, 2001. These tests were intended to verify that the closed loop controllers were capable of precise line following with the increased disturbances due to the wing-sail propulsion. System identification for the controller design was obtained previously using a trolling motor as the propulsion system, in place of the wing-sail which was still under construction. No modifications were made to the LQR controller design, and the tests were run on a day with approximately 10 knots (or 5 m/s) of wind, with gusts up to the 16 knot (or 8 m/s) range.

Upon analyzing the data, it was demonstrated that the Atlantis was capable of sailing to within 25 degrees of the true wind direction. Fig. 2 presents a close-up of the first path of regulated control, and looks at the cross-track error (Y), azimuth error (Ψ), and velocities (V). Note that the dark line in the top of the velocity graph is the wind speed, and can be seen to vary well over 50% of nominal.

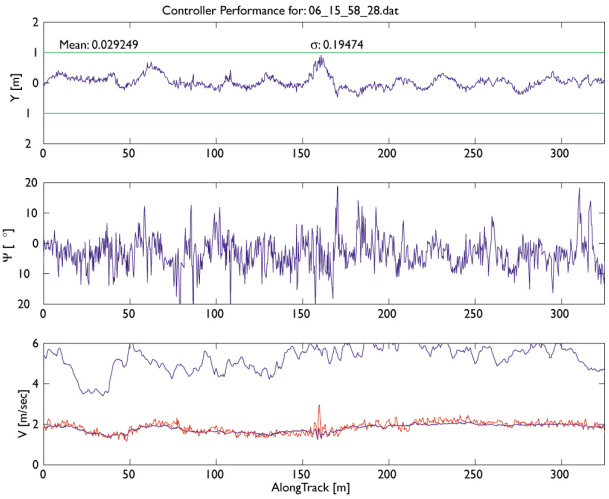

Fig. 2. Sailing path errors.

The mean of the cross-track error is less than 3 cm., and the standard deviation is less than 30 cm., note that this is the Sailboat Technical Error (STE, the sailing analog of Flight Technical Error). Previous characterization of the coast-guard differential GPS receiver indicated that the Navigation Sensor Error (NSE) is approximately 36 cm., thus the Total System Error (TSE) is less than 1 meter

$$\text{TSE} = \text{STE} + \text{NSE}. \tag{1}$$

III. Model Free Subspace $\mathcal{H}_\infty$ Control

A. Introduction

Subspace system identification methods have recently become popular for the identification of linear time invariant (LTI) systems. Initially, experimental data is used to derive a least squares optimal predictor. The predictor can then be used to derive a state space model of the dynamic system. This derivation of the state space model from the predictor can be thought of as plant model order reduction. Instead of using this reduced order model for control design, model free control performs the control design directly from the subspace

predictor, avoiding the formal model formation step in the design process.

Model free subspace $\mathcal{H}_\infty$ control exploits this subspace prediction method to provide a direct $\mathcal{H}_\infty$ control design technique. A single, integrated algorithm computes the $\mathcal{H}_\infty$-optimal controller and provides an estimate of the closed loop performance. For a more thorough discussion of subspace prediction and the model free subspace $\mathcal{H}_\infty$ controller see [14], [15].

Fig. 3 provides an overview of the model free subspace $\mathcal{H}_\infty$ control design procedure. Open loop experimental data is initially used to calculate a high order predictor. System performance specifications are defined using the weighting functions W_1 and W_2. The predictor and control parameters are then combined to form the controller.

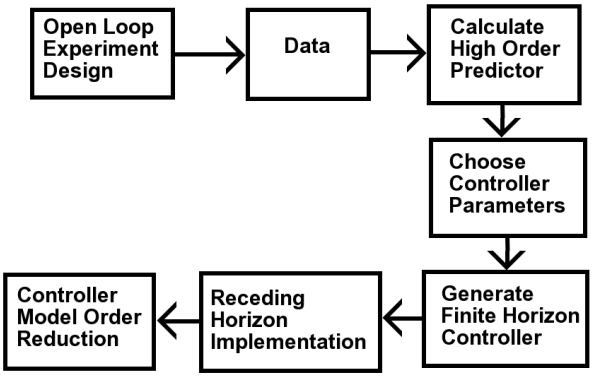

Fig. 3. Model free subspace $\mathcal{H}_\infty$ control design.

The model free subspace based $\mathcal{H}_\infty$ control law utilizes a finite horizon cost function and is implemented with a "receding horizon" procedure. In this form, the control law is a member of a general class of controllers known as predictive control. Using a future horizon of length i, at the time k the optimal control u_{opt} is calculated. The control at time k is then implemented and data y_k and r_k are collected. The "horizon" is then shifted one step into the future and the procedure is repeated. The Atlantis uses a simple LTI discrete time system to express the receding horizon controller implementation. Standard model order reduction tools can then be applied to the LTI discrete time system if appropriate.

The reduction of the system identification step allows for an adaptive controller implementation that can adjust its performance specification as new closed loop input-output data is obtained. This adaptive implementation [16] will not be explored in this paper, although its existence offers substantial motivation for the application of these model free techniques.

As expected, the receding horizon controller implementation is derived from the $\mathcal{H}_\infty$ performance specification and the subspace predictor. The control design procedure can however, be viewed as a "black box" requiring the following steps:

1) Collect experimental data.
2) Select i,j, and weighting functions W_1,W_2.
3) Compute γ_{min} and reselect W_1,W_2 if necessary (ideally $\gamma_{min} \leq 1$). Finalize the choice of W_1, W_2 and choose $\gamma > \gamma_{min}$.
4) Compute and implement the final $i(m+l) + n_{w_1} + n_{w_2}$ order LTI control law and apply controller order reduction if necessary.

The following subsections outline the key elements of this novel control design technique. An in depth analysis of $\mathcal{H}_\infty$ control, including its advantages over $\mathcal{H}_2$ techniques, can be found in [7].

B. Subspace Prediction

Consider data of length n from a MIMO plant where $u_k \in \mathbb{R}^m$ and $y_k \in \mathbb{R}^l$, m are the number of inputs, and l are the number of outputs. A subspace predictor can be generated from this data by choosing a specific prediction horizon, i, that is larger than the expected order of the LTI plant. This prediction horizon is then used to break the data set into j prediction problems, where $j = n-2i+1$ and $j \gg i$. These j prediction problems are then used to generate the least squares optimal predictor $L_w \in \mathbb{R}^{il \times i(l+m)}$ and $L_u \in \mathbb{R}^{il \times im}$.

Using k as the present time index, we can then use L_w and L_u to predict future outputs given past experimental data and future inputs

$$\begin{bmatrix} \hat{y}_k \\ \vdots \\ \hat{y}_{k+i-1} \end{bmatrix} = L_w \begin{bmatrix} u_{k-i} \\ \vdots \\ u_{k-1} \\ y_{k-i} \\ \vdots \\ y_{k-1} \end{bmatrix} + L_u \begin{bmatrix} u_k \\ \vdots \\ u_{k+i-1} \end{bmatrix} \tag{2}$$

The derivation of L_w and L_u is reasonably straight forward. First, we define block Hankel matrices from the data using the subscript "p" to represent "past" data and "f" to represent the corresponding "future" data

$$U_p \triangleq \begin{bmatrix} u_0 & u_1 & \dots & u_{j-1} \\ u_1 & u_2 & \dots & u_j \\ \vdots & \vdots & \dots & \vdots \\ u_{i-1} & u_i & \dots & u_{i+j-2} \end{bmatrix} \in \mathbb{R}^{im \times j} \tag{3}$$

$$U_f \triangleq \begin{bmatrix} u_i & u_{i+1} & \dots & u_{i+j-1} \\ u_{i+1} & u_{i+2} & \dots & u_{i+j} \\ \vdots & \vdots & \dots & \vdots \\ u_{2i-1} & u_{2i} & \dots & u_{2i+j-2} \end{bmatrix} \in \mathbb{R}^{im \times j} \tag{4}$$

$$Y_p \triangleq \begin{bmatrix} y_0 & y_1 & \dots & y_{j-1} \\ y_1 & y_2 & \dots & y_j \\ \vdots & \vdots & \dots & \vdots \\ y_{i-1} & y_i & \dots & y_{i+j-2} \end{bmatrix} \in \mathbb{R}^{il \times j} \tag{5}$$

$$Y_f \triangleq \begin{bmatrix} y_i & y_{i+1} & \dots & y_{i+j-1} \\ y_{i+1} & y_{i+2} & \dots & y_{i+j} \\ \vdots & \vdots & \dots & \vdots \\ y_{2i-1} & y_{2i} & \dots & y_{2i+j-2} \end{bmatrix} \in \mathbb{R}^{il \times j} \tag{6}$$

All past data can then be combined as

$$W_p \triangleq \begin{bmatrix} U_p \\ Y_p \end{bmatrix} \tag{7}$$

Obtaining the best linear least squares predictor of Y_p given W_p and U_f can be formed as the Frobenius norm minimization

$$\min_{L_w, L_u} \left\| Y_f - \begin{bmatrix} L_w & L_u \end{bmatrix} \begin{bmatrix} W_p \\ U_f \end{bmatrix} \right\|_F^2 \tag{8}$$

The solution to this optimization problem is now given by the orthogonal projection of the row space of Y_f into the row space spanned by W_p and U_f. This orthogonal projection solution to (8) is given as

$$\hat{Y}_f = Y_f \Big/ \begin{bmatrix} W_p \\ U_f \end{bmatrix} \tag{9}$$

$$\triangleq Y_f \begin{bmatrix} W_p \\ U_f \end{bmatrix}^T \left(\begin{bmatrix} W_p \\ U_f \end{bmatrix} \begin{bmatrix} W_p \\ U_f \end{bmatrix}^T \right)^\dagger \begin{bmatrix} W_p \\ U_f \end{bmatrix} \tag{10}$$

where $\dagger$ denotes the Moore-Penrose or pseudoinverse. Therefore

$$\begin{bmatrix} L_w & L_u \end{bmatrix} = Y_f \begin{bmatrix} W_p \\ U_f \end{bmatrix}^T \left(\begin{bmatrix} W_p \\ U_f \end{bmatrix} \begin{bmatrix} W_p \\ U_f \end{bmatrix}^T \right)^\dagger \tag{11}$$

C. Model Free Subspace $\mathcal{H}_\infty$ Control

The subspace predictor of the previous subsection will now be utilized to derive a finite-horizon, model free, subspace based, $\mathcal{H}_\infty$-optimal feedback controller. An $\mathcal{H}_\infty$ mixed sensitivity criteria is used to specify the desired minimum control performance and desired maximum control usage. Assuming a discrete time output unity feedback structure the specification used is

$$\left\| \begin{bmatrix} W_1 S \\ W_2 Q \end{bmatrix} \right\|_\infty \leq \gamma \tag{12}$$

where

$$S = (I + PK)^{-1} = G_{er} \tag{13}$$

$$Q = K(I + PK)^{-1} = G_{ur} \tag{14}$$

for some plant P and controller K, and W_1 and W_2 are weighting functions chosen to provide the desired system performance. Small S up to a desired cutoff frequency corresponds to each output tracking its reference well in the frequencies of interest. Limiting the magnitude of Q, especially at high frequencies, limits the control effort used.

The time-domain discrete-time expression for the specification in (12) is formulated as follows:

$$z \triangleq \begin{bmatrix} z_{w1} \\ z_{w2} \end{bmatrix} = \begin{bmatrix} w_1 * e \\ w_2 * u \end{bmatrix} = \begin{bmatrix} w_1 * (r - y) \\ w_2 * u \end{bmatrix} \tag{15}$$

where w_1 and w_2 are the respective discrete impulse responses of the discrete time weighting functions W_1 and W_2. Using (15), the finite-horizon problem of (12) can be written as

$$\sup_r J(\gamma) \leq 0, \text{ where } J(\gamma) = \sum_{t=0}^{i-1} (z_t^T z_t - \gamma^2 r_t^T r_t) \tag{16}$$

and the system is assumed to be at rest at $t = 0$. The length of the horizon, i, has been selected to be identical to the prediction horizon in the previous subsection, so (2) can be used to calculate $J(\gamma)$. Using $J(\gamma)$ from (16), the central finite-horizon $\mathcal{H}_\infty$ controller satisfies

$$\min_u \sup_r J(\gamma) \leq 0 \tag{17}$$

whenever the system is at rest at $t = 0$.

D. Subspace Based finite-horizon $\mathcal{H}_\infty$ Control

Given the generalized plant of Fig. 4, the level-γ $\mathcal{H}_\infty$ control design problem is to choose a control u such that the finite-horizon $\mathcal{H}_\infty$ gain from r to z is of magnitude γ. This subsection derives the condition on γ that ensures that the problem is feasible, and computes the central solution for this $\mathcal{H}_\infty$ control problem.

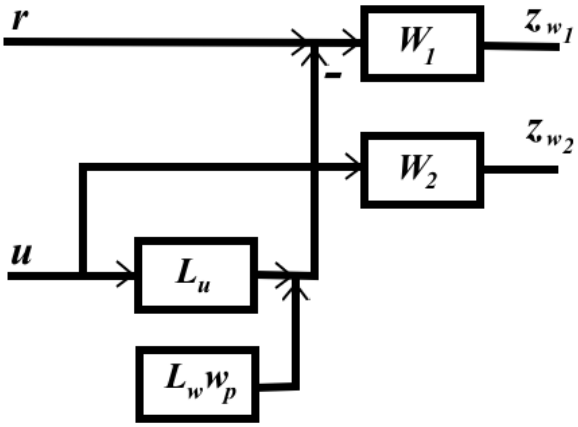

Fig. 4. Generalized plant for $\mathcal{H}_\infty$ control design.

If measurements of the plant input u, plant output y, and reference r are available for times $\{k-i, \ldots, k-2, k-1\}$, then the strictly causal, finite-horizon, model free, subspace based, level-γ, central $\mathcal{H}_\infty$ control for times $\{k, \ldots, k+i-1\}$ is

$$u_{opt} = -(L_u^T \tilde{Q}_1 L_u + Q_2)^{-1} \cdot \begin{bmatrix} (L_u^T \tilde{Q}_1 L_w)^T \\ \left(-L_u^T (\gamma^{-2} \tilde{Q}_1 + I) H_1^T \Gamma_1 \right)^T \\ (H_2^T \Gamma_2)^T \end{bmatrix}^T \begin{bmatrix} w_p \\ x_{w_1} \\ x_{w_2} \end{bmatrix}_k \tag{18}$$

$$\tilde{Q}_1 = (Q_1^{-1} - \gamma^{-2} I)^{-1} \tag{19}$$

provided that

$$\gamma > \gamma_{min} \triangleq \sqrt{\overline{\lambda}[(Q_1^{-1} + L_u Q_2^{-1} L_u^T)^{-1}]} \tag{20}$$

where the discrete LTI weighting filters W_1 and W_2 have the minimal state space representation

$$(x_{w_1})_{k+1} = A_{w_1}(x_{w_1})_k + B_{w_1}(r_k - y_k) \tag{21}$$
$$(z_{w_1})_k = C_{w_1}(x_{w_1})_k + D_{w_1}(r_k - y_k) \tag{22}$$
$$(x_{w_2})_{k+1} = A_{w_2}(x_{w_2})_k + B_{w_2}(u_k) \tag{23}$$
$$(z_{w_2})_k = C_{w_2}(x_{w_2})_k + D_{w_2}(r_k - y_k) \tag{24}$$

The lower triangular Toeplitz matrices H_1 and H_2 are formed from the Markov parameters of the discrete weighting filters W_1 and W_2

$$H_1 \triangleq \begin{bmatrix} D_{w_1} & \dots & 0 & \dots & 0 \\ C_{w_1}B_{w_1} & \dots & 0 & \dots & 0 \\ C_{w_1}A_{w_1}B_{w_1} & \dots & D_{w_1} & \dots & 0 \\ \vdots & \vdots & \ddots & \vdots & \\ C_{w_1}A_{w_1}^{i-2}B_{w_1} & \dots & C_{w_1}A_{w_1}^{i-4}B_{w_1} & \dots & D_{w_1} \end{bmatrix} \tag{25}$$

$$H_2 \triangleq \begin{bmatrix} pD_{w_2} & \dots & 0 & \dots & 0 \\ C_{w_2}B_{w_2} & \dots & 0 & \dots & 0 \\ C_{w_2}A_{w_2}B_{w_2} & \dots & D_{w_2} & \dots & 0 \\ \vdots & \vdots & \ddots & \vdots & \\ C_{w_2}A_{w_2}^{i-2}B_{w_2} & \dots & C_{w_2}A_{w_2}^{i-4}B_{w_2} & \dots & D_{w_2} \end{bmatrix} \tag{26}$$

and

$$Q_1 \triangleq H_1^T H_1 \ , \ Q_2 \triangleq H_2^T H_2 \tag{27}$$

The extended observability matrices that contain the weighting filter impulse responses are defined as

$$\Gamma_1 \triangleq \begin{bmatrix} C_{w_1} \\ C_{w_1}A_{w_1} \\ \vdots \\ C_{w_1}A_{w_1}^{i-1} \end{bmatrix} \ , \ \Gamma_2 \triangleq \begin{bmatrix} C_{w_2} \\ C_{w_2}A_{w_2} \\ \vdots \\ C_{w_2}A_{w_2}^{i-1} \end{bmatrix} \tag{28}$$

and vector of past plant inputs and outputs is defined as

$$(w_p)_k \triangleq \begin{bmatrix} u_{k-i} \\ \vdots \\ u_{k-1} \\ y_{k-i} \\ \vdots \\ y_{k-i} \end{bmatrix}. \tag{29}$$

E. MFS$\mathcal{H}_\infty$ Predictive Control

The final step of the control design procedure, the receding horizon implementation, is expressed as the following MIMO LTI discrete time system :

$$\begin{bmatrix} u_p \\ y_p \\ x_{w_1} \\ x_{w_1} \end{bmatrix}_{k+1} = \begin{bmatrix} \begin{bmatrix} S_m \\ k_1 \end{bmatrix} & \begin{bmatrix} 0 \\ k_2 \end{bmatrix} & \begin{bmatrix} 0 \\ k_3 \end{bmatrix} & \begin{bmatrix} 0 \\ k_4 \end{bmatrix} \\ 0 & \begin{bmatrix} S_l \\ 0 \end{bmatrix} & 0 & 0 \\ 0 & 0 & A_{w_1} & 0 \\ B_{w_2}k_1 & B_{w_2}k_2 & B_{w_2}k_3 & A_{w_2} + B_{w_2}k_4 \end{bmatrix} \begin{bmatrix} u_p \\ y_p \\ x_{w_1} \\ x_{w_1} \end{bmatrix}_k + \begin{bmatrix} 0 & 0 \\ 0 & \begin{bmatrix} 0 \\ I_l \end{bmatrix} \\ B_{w_1} & B_{w_1} \\ 0 & 0 \end{bmatrix} \begin{bmatrix} r \\ y \end{bmatrix}_k \tag{30}$$

$$u_k = \begin{bmatrix} k_1 & k_2 & k_3 & k_4 \end{bmatrix} \begin{bmatrix} u_p \\ y_p \\ x_{w_1} \\ x_{w_2} \end{bmatrix}_k \tag{31}$$

where $u_k \in \mathbb{R}^m$, $r_k \in \mathbb{R}^l$, $y_k \in \mathbb{R}^l$, m are the number of plant inputs, and l are the number of plant outputs. I_m and I_l are defined as $m \times m$ and $l \times l$ identity matrices respectively,

$$S_m = \begin{bmatrix} 0 & I_m & 0 & \dots & 0 \\ 0 & 0 & I_m & \dots & 0 \\ \vdots & \vdots & \vdots & \ddots & 0 \\ 0 & 0 & 0 & \dots & I_m \end{bmatrix} \in \mathbb{R}^{(i-1)m \times im} \tag{32}$$

$$S_l = \begin{bmatrix} 0 & I_l & 0 & \dots & 0 \\ 0 & 0 & I_l & \dots & 0 \\ \vdots & \vdots & \vdots & \ddots & 0 \\ 0 & 0 & 0 & \dots & I_l \end{bmatrix} \in \mathbb{R}^{(i-1)l \times il} \tag{33}$$

and

$$\begin{bmatrix} k_1 & k_2 \end{bmatrix} = \left\{ -(L_u^T \tilde{Q}_1 L_u + Q_2)^{-1} L_u^T \tilde{Q}_1 L_w \right\}_{1:m,:} \tag{34}$$

$$k_3 = \left\{ (L_u^T \tilde{Q}_1 L_u + Q_2)^{-1} L_u^T (\gamma^{-2}\tilde{Q}_1 + I) H_1^T \Gamma_1 \right\}_{1:m,:} \tag{35}$$

$$k_4 = \left\{ -(L_u^T \tilde{Q}_1 L_u + Q_2)^{-1} H_2^T \Gamma_2 \right\}_{1:m,:} \tag{36}$$

where $\{\bullet\}_{1:m,:}$ means extract the first m rows of the matrix $\bullet$, and $k_1 \in \mathbb{R}^{m \times im}$, $k_2 \in \mathbb{R}^{m \times il}$, $k_3 \in \mathbb{R}^{m \times n_{w_1}}$, $k_4 \in \mathbb{R}^{m \times n_{w_2}}$.

IV. Atlantis Controller Design Parameters

A. Subspace Prediction Horizon

As discussed in Section III, the subspace predictor is generated using experimental input-output data of length n. A prediction horizon, i, is then chosen that breaks the data set into j prediction problems, where $j = n - 2i + 1$. To ensure an accurate predictor is created for a LTI model, i will be chosen to be at least twice as large the expected plant order.

The simulated system identification data used to generate the subspace predictor is shown in Fig. 5. The boat uses rudder

slew rate ($\dot{\delta}$) as the input signal and has three output signals: cross-track (Y), azimuth (Ψ), and effective rudder angle (δ).

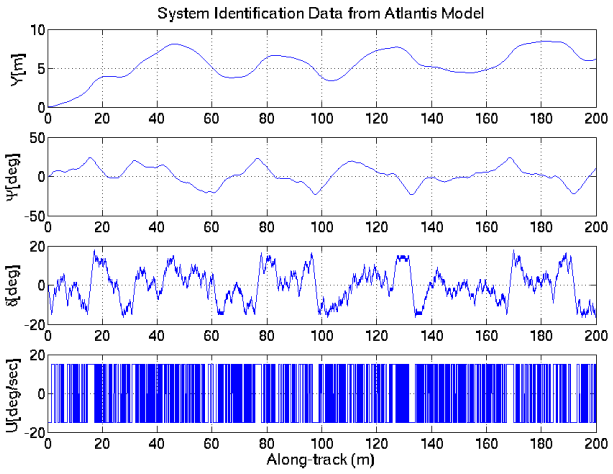

Fig. 5. Simulated open loop system identification data created by controlling the slew rate of the Atlantis with a pseudo-random binary sequence.

Although the Atlantis is a nonlinear system, Section II shows that LQG techniques are effective for precision control when small azimuth and cross-track deviations are maintained. To generate a more accurate predictor a high order prediction horizon was used by choosing $i = 100$. Fig. 6 shows the predictor generated is adequate at predicting Atlantis' response to a known input. This particular data was from a simulated system identification pass similar to that shown in Fig. 5, however, this data was not used in generating the subspace predictor.

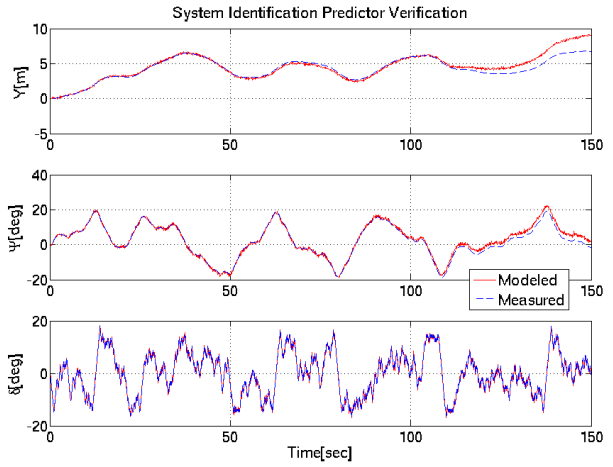

Fig. 6. The subspace predictor reconstruction of a simulated system identification pass comparing measured outputs to predicted values.

B. Mixed Sensitivity Cost Function

As shown in Section III, W_1 and W_2 are weighting functions chosen to provide the desired system performance for the mixed sensitivity criteria given in (12). It is important to note that increasing either the DC gain or bandwidth of W_1 will make the controller more aggressive. This will force the controller to track higher error signal frequencies making the response faster, but less damped. Decreasing W_2 will permit greater control usage, which is typically not desirable at high frequencies. However, if W_1 is increased, requesting higher performance, but W_2 is not sufficiently decreased, to provide more control usage, the problem will become over constrained. These over lapping constraints will be reflected by γ_{opt} increasing over the nominal value of one. W_1 and W_2 were then selected with these performance tradeoffs in mind.

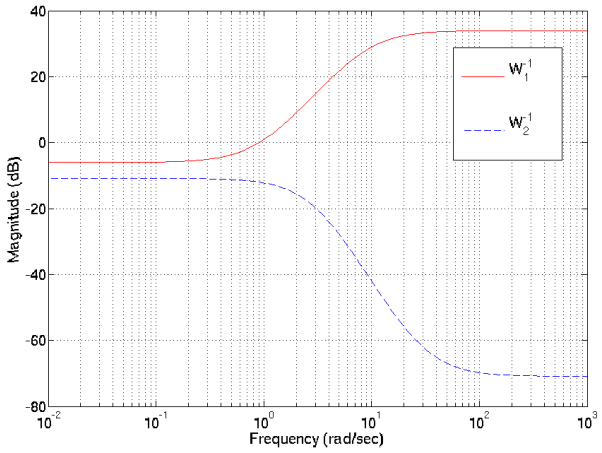

Fig. 7. Control Specification for Atlantis. Note all three control inputs use the identical cost function W_1^{-1}.

Fig. 7 shows the inverse of each weighting function chosen for the Atlantis. Identical W_1 functions were used to specify the performance requirements for Y, Ψ, and δ. As shown, the design cutoff frequency is around 0.9 rad/sec (0.14 Hz). It is desirable that all three outputs stay nominally around zero to provide a more linear response of the system, therefore 6 dB of rejection at DC was chosen. The control usage function, W_2, which effects the slew rate of the rudders was then selected to provide sufficient control usage to meet the performance specifications while staying within the limitations of the rudder actuator system.

A value of γ was selected that would provide fairly aggressive closed loop response while allowing some margin to maintain stability. The smallest achievable γ value, γ_{min}, was calculated to be 1.81 based on the previously described predictor and weighting functions. We then chose $\gamma = (1.5)\gamma_{min} = 2.71$ which is later shown to meet our controller requirements.

C. Model Order Reduction

Initially, a high order predictor was used to provide as much information as possible for the controller design. The controller generated using the high order subspace predictor therefore also had a substantially high order. Fig. 8 shows the Hankel singular values of the controller generated from the subspace predictor, weighting functions, and γ value.

The first five singular values of the Hankel matrix stand out, therefore it is assumed the controller can be reduced

to a fifth order system. A balanced realization was then used to truncate the controller at the desired order. This assumption was verified by simulating controllers of various orders. Results showed that keeping modes higher than five did not noticeably effect system performance.

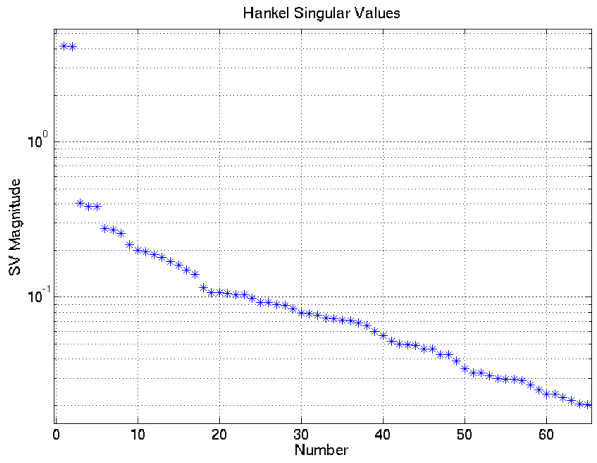

Fig. 8. Hankel Singular Value plot of initial controller design. Note the drop off in the singular values after the fifth one, indicating a system of order five.

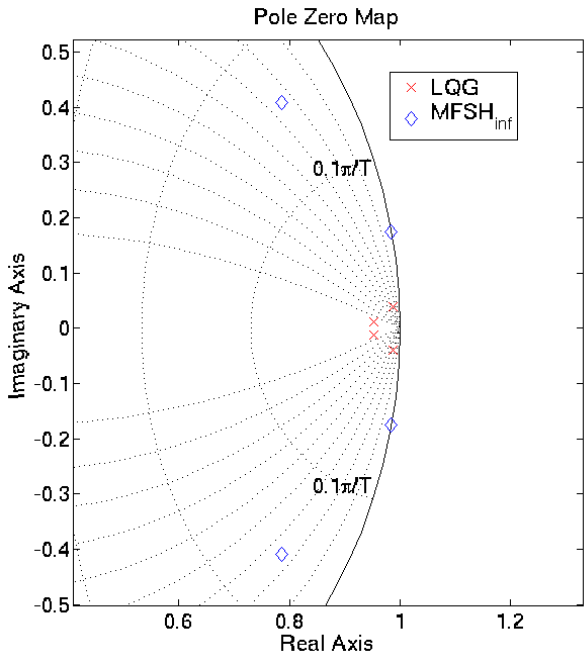

Fig. 9. Mapping of poles for LQG (red) and MFS$\mathcal{H}_\infty$ (blue) controllers created from experimental system identification data.

V. Comparison of LQG and MFS$\mathcal{H}_\infty$ Controllers

Two unique controllers developed from experimental system identification data similar to Fig. 5 are now compared. The first controller uses the OKID method to generate a LTI model of the plant. As previously described in Section II, an LQG controller was created from the OKID model. The model free subspace $\mathcal{H}_\infty$ controller described in Section III was then applied using the same system identification data and the design parameters discussed in Section IV.

A mapping of the poles for both controllers is shown in Fig. 9. From this, we can see that the model free subspace $\mathcal{H}_\infty$ controller has a bandwidth at significantly higher frequency then the LQG controller. This is expected, because the MFS$\mathcal{H}_\infty$ controller is frequency agnostic and will move up in frequency to achieve higher performance routinely. In terms of damping, the MFS$\mathcal{H}_\infty$ controller appears to be less damped than the LQG, which again is consistent with the formulation.

A bode plot showing the frequency response of $\frac{\delta(j\omega)}{Y(j\omega)}$ for both controllers is provided in Fig. 10. The MFS$\mathcal{H}_\infty$ controller shows a DC gain of -25dB, which corresponds with the specifications as shown in Fig. 7, and again shows a propensity for higher frequency excitation than the LQG.

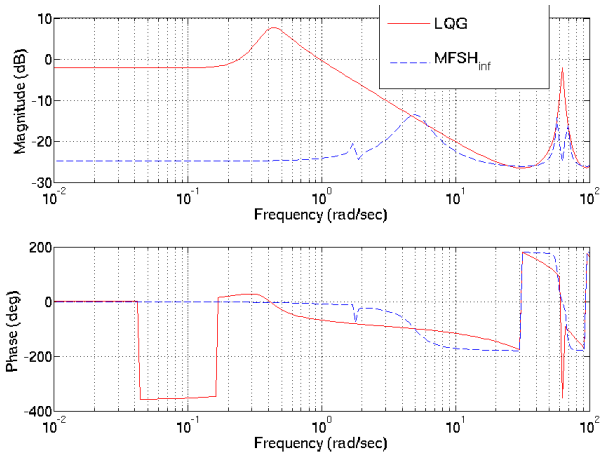

Fig. 10. Bode plot of LQG (red) and MFS$\mathcal{H}_\infty$ (blue) controllers created from experimental system identification data.

VI. Segmented Trajectory Generation Using Arcs and Lines

The way-point navigation system uses a series of user defined way-points as reference points for navigation. The Atlantis could simply use these way-points as heading references, however large cross-track errors would be produced during way-point transitions and certain references may be unreachable because of the wind direction. A segmented trajectory of lines connected by arcs of a constant radius is used to provide achievable trajectory paths.

Arc segments are added between line segments such that the line segments are tangent to the arc where they meet, providing a smooth transition point between segments. Fig. 11 demonstrates how way-point inputs are transformed to line and arc segments. In practice, segments will be created in real-time as way-points are achieved allowing for tacking scenarios to be applied when necessary.

When the Atlantis transitions from tracking a line segment to an arc, a feedforward component providing the proper nominal rudder angle is added to the rudder control signal. The separate closed loop line following controller then stabilizes

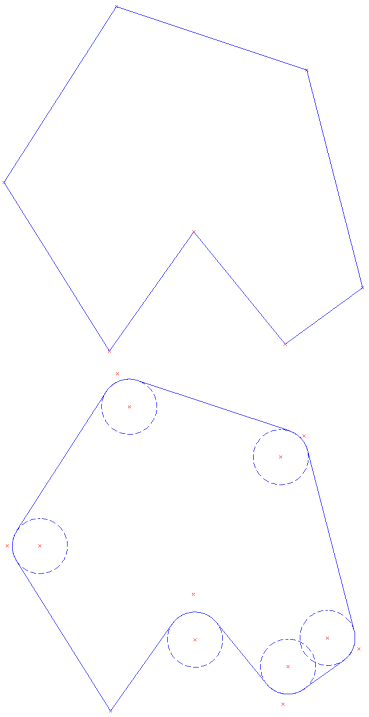

Fig. 11. User defined way-points (top) transformed into arc and line segments (bottom).

the system around this nominal rudder angle for a given turning radius. The feedforward term is removed once the arc is traversed and the new line segment is being tracked.

VII. Simulation Results

A nonlinear model of the Atlantis which includes wind and wave disturbances was previously developed in [2]. This model, combined with the way-point navigation system described in Section VI was then used in Monte Carlo simulations to compare three different controllers designed for precise trajectory tracking in the presence of environmental disturbances. Each controller monitors azimuth (Ψ), cross-track (Y), and rudder position (δ) to adjust the rudder slew rate ($\dot{\delta}$). The first controller simulated is the PID controller described in [2]. Next the LQG controller developed in [1] was simulated. Finally, the model free subspace $\mathcal{H}_\infty$ controller developed in Section IV was tested.

The set of way-points shown in Fig. 12 were selected and Monte Carlo simulations were run for 100,000 seconds for each of the three different controllers, with random wind and water disturbance conditions provided for each trial. The results obtained are shown in Table I, the model free subspace $\mathcal{H}_\infty$ controller obtained the smallest combination of total average cross-track error and cross-track error standard deviation. Fig. 13 shows the resulting cross-track and azimuth error data from an average simulated run. Monte Carlo simulation results show the Atlantis having an average cross-track error of 8 cm with a standard deviation of 65 cm when using the model free subspace $\mathcal{H}_\infty$ controller.

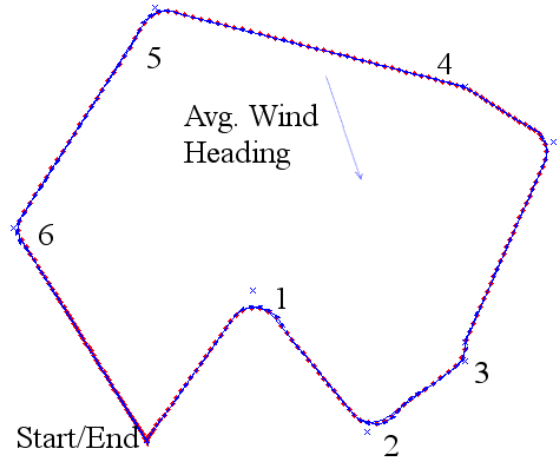

Fig. 12. Control architecture applied to wing-sailed vehicle simulated with water current and wave disturbances.

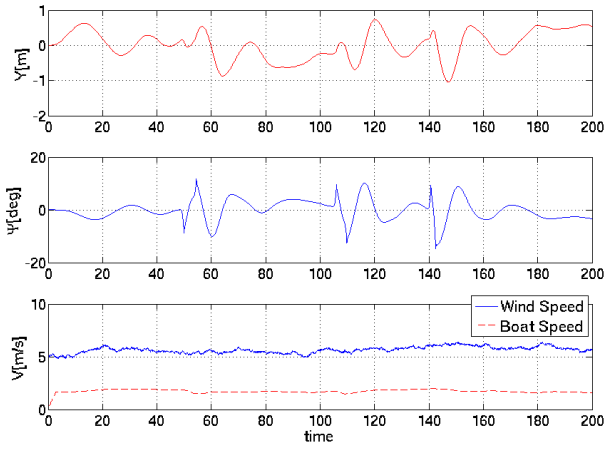

Fig. 13. Azimuth and cross-track error for wing-sailed surface vehicle simulation.

TABLE I
Simulation Results.

	PID		LQG		MFS$\mathcal{H}_\infty$	
	Lines	Total	Lines	Total	Lines	Total
$\overline{Y}$(cm)	20	27	1	8	2	8
Y_σ(cm)	49	59	61	75	56	65
$\overline{Y} + Y_\sigma$(cm)	69	86	62	84	58	73

Analysis of the simulation results shows that all three controllers perform comparably for straight line segments. However, the disturbances introduced by the addition of arc segments produced greater errors for the PID and LQG controllers. The MFS$\mathcal{H}_\infty$ controller performed more than 10% better than the other controllers within the complete segmented trajectory guidance system, even though considerably less tuning of control parameters was necessary for the MFS$\mathcal{H}_\infty$ controller.

VIII. Conclusions

A control architecture for an autonomous sailboat using a way-point navigation system was simulated using a model free subspace $\mathcal{H}_\infty$ controller and shown capable of providing robust and reliable guidance under realistic wind and water disturbance models. This architecture was applied to a simplified model of the Atlantis, a wing-sail propelled catamaran previously shown capable of line following accuracy better than 0.3 meters. Simulations modeling similar experimental conditions previously encountered show that precision control is possible for way-point navigation requiring segmented trajectory following of arcs and lines and real-time way-point management to prevent unreachable points of sail.

Simulations show the sailboat can be controlled to better than one meter of accuracy, providing similar performance to previous experimental results using an LQG controller. However, a key difference is the model free subspace $\mathcal{H}_\infty$ controller reduces the complexity of the control design process by eliminating the standard model formation step. This direct control design methodology has also been demonstrated to perform exceptionally well when used in an adaptive controller implementation. Application of this adaptive control technique will be the focus of future precision control research for the Atlantis. Experimental validation is expected within the next year.

Other future work will include a way-point generation methodology that will avoid stationary obstacles and also optimally determine trajectories given only a destination point and weather data forecasts to predict future wind and wave activity. This added guidance system combined with advancements in Atlantis sensors and actuators will create a wind-propelled ASV capable of robust navigation.

References

[1] G.H. Elkaim. *System Identification for Precision Control of a Wingsailed GPS-Guided Catamarn*. PhD thesis, Stanford University, 2001.

[2] G.H. Elkaim and R.J. Kelbley. Control architecture for segmented trajectory following of a wind-propelled autonomous catamaran. *AIAA Guidance, Navigation, and Control Conference*, August 2006.

[3] P. Encarnacao, A. Pascoal, and M. Arcak. Path following for autonomous marine craft. *5th IFAC Conference on Maneuvering and Control of Marine Craft*, pages 117–22, 2000.

[4] T.I. Fossen. *Guidance and Control of Ocean Vehicles*. Wiley and Sons, New York, NY, 1994.

[5] M. Gevers. Identification for control: From the early achievements to the revival of experiment design. *European Journal of Control*, 11:335–352, 2005.

[6] J.-N. Juang. *Applied System Identification*. Prentice Hall, NJ, 1994.

[7] K.Zhou. *Robust and Optimal Control*. Prentice-Hall, Inc., Upper Saddle River, NJ, 1996.

[8] E. Lefeber, KY. Pettersen, and H. Nijmeijer. Tracking control of an underactuated ship. *IEEE Transactions on Control Systems Technology*, 3:52–61, January 2003.

[9] B.W. McCormick. *Aerodynamics, Aeronautics, and Flight Mechanics*. John Wiley and Sons, New York, NY, 1979.

[10] A. Pascoal, P. Olivera, and C. Silvestre. Robotic ocean vehicles for marine science applications: The european asimov project. *OCEANS 2000 MTS/IEEE Conference and Exhibition*, 1:409–415, 2000.

[11] R.S.Shevell. *Fundamentals of Flight*. Prentice-Hall, Inc., Englewood Cliffs, NJ, 1983.

[12] R. Skjetne and T. Fossen. Nonlinear maneuvering and control of ships. *MTS/IEEE OCEANS 2001*, 3:1808–15, 2001.

[13] T. VanZwieten. *Dynamic Simulation and Control of an Autonomous Surface Vehicle*. PhD thesis, Florida Atlantic University, 2003.

[14] B.R. Woodley. *Model Free Subspace Based $\mathcal{H}_\infty$ Control*. PhD thesis, Stanford University, 2001.

[15] B.R. Woodley, J.P. How, and R.L. Kosut. Model free subspace based $\mathcal{H}_\infty$ control. *Proceedings of the American Control Conference*, pages 2712–2717, 2001.

[16] B.R. Woodley, J.P. How, and R.L. Kosut. Subspace based direct adaptive $\mathcal{H}_\infty$ control. *Int. J. Adapt. Control Signal Process*, 15:535–561, 2001.